

Impact of Kinematics, Microphysics, and Electrification on the Formation of Lightning-Weak Holes in a Simulated Supercell Storm

Conrad L. Ziegler^{1*}, Edward R. Mansell¹, Kristin M. Calhoun^{1,2}, and Donald R. MacGorman¹

1. National Severe Storms Laboratory (NSSL), Norman, Oklahoma, USA

2. Cooperative Institute for Mesoscale Meteorological Studies, University of Oklahoma, Norman, Oklahoma, USA

ABSTRACT: This study investigates the impact of evolving kinematics, microphysics, and electrification on the development of lightning-weak holes (LWH) in a simulated supercell storm. The first 6 hours of evolution of the tornadic supercell storm near Geary, Oklahoma, USA on 29-30 May 2004 are simulated with NSSL's three-dimensional COMMAS cloud model. We explore the hypothesis that development of the low-level mesocyclone (LLM) injects graupel-meltwater rain via the radar "hook-echo" into the base of the main updraft, leading to rapid vertical rainwater advection and midlevel freezing to form riming graupel that subsequently fills the BWER and initiates noninductive graupel-ice charging. We further hypothesize that as the mixed-phase BWER fills with charging graupel, new charge centers begin forming in the midlevel updraft that subsequently support both lightning flash initiation and leader propagation into those new charge centers.

1. INTRODUCTION

The electrical property of strong and supercell storms known as the "lightning-weak hole" (LWH) has generated increasing interest in recent years, as the development of the Lightning Mapping Array (LMA) technology by the New Mexico Institute of Mining and Technology and newly-deployed LMA systems in supercell-prone areas have led to increasing observations of this enigmatic storm electrical phenomenon. The morphology and possible charging mechanisms that support the development of supercell LWHs have been investigated by Krehbiel et al. (2000), MacGorman et al. (2005), Payne et al. (2005), Steiger et al. (2007), and Calhoun et al. (2013, 2014). For improved consistency with the supercell storm's morphology as described by the conventional radar-based terminology for the bounded weak echo region (BWER), we will subsequently refer to the lightning-weak hole as a "bounded weak lightning region" or "BWLR". For comparison with previous studies of the tornadic 29-30 May 2004 Geary, Oklahoma, USA supercell storm by Calhoun et al. (2013, 2014), the present study conducts a detailed simulation of the Geary supercell with NSSL's three-dimensional COMMAS cloud model. We will examine the simulated storm to identify BWLRs and identify the ambient cloud conditions that associate with modeled BWLRs.

The Geary supercell storm contained several transient BWLRs in proximity to its main updraft and BWER, as previously documented with radar and Oklahoma LMA observations and Ensemble Kalman Filter (EnKF) analyses (Calhoun et al. 2013, Calhoun et al. 2014). We will explore the hypothesis that the BWLR is associated with regions of the supercell storm that contain weak hydrometeor and net space charges, including BWERs but more generally regions containing either small net charges or else cloud and precipitation particles that individually experience little or no charging along their trajectories. We will also explore the corollary hypothesis that graupel and graupel-meltwater are entrained into the main updraft via the radar "hook-echo" and mesocyclone stimulate vertical advection, subsequently leading to redevelopment of riming graupel within the in-filled BWER, invigoration of noninductive graupel-ice charging, generation new net charge centers, and ultimately to renewed lightning activity within the main updraft where a BWLR may have recently existed.

* Corresponding author, Email: conrad.ziegler@noaa.gov, Postal address: NSSL, 120 David L. Boren Blvd., Norman, OK 73072 U.S.A.

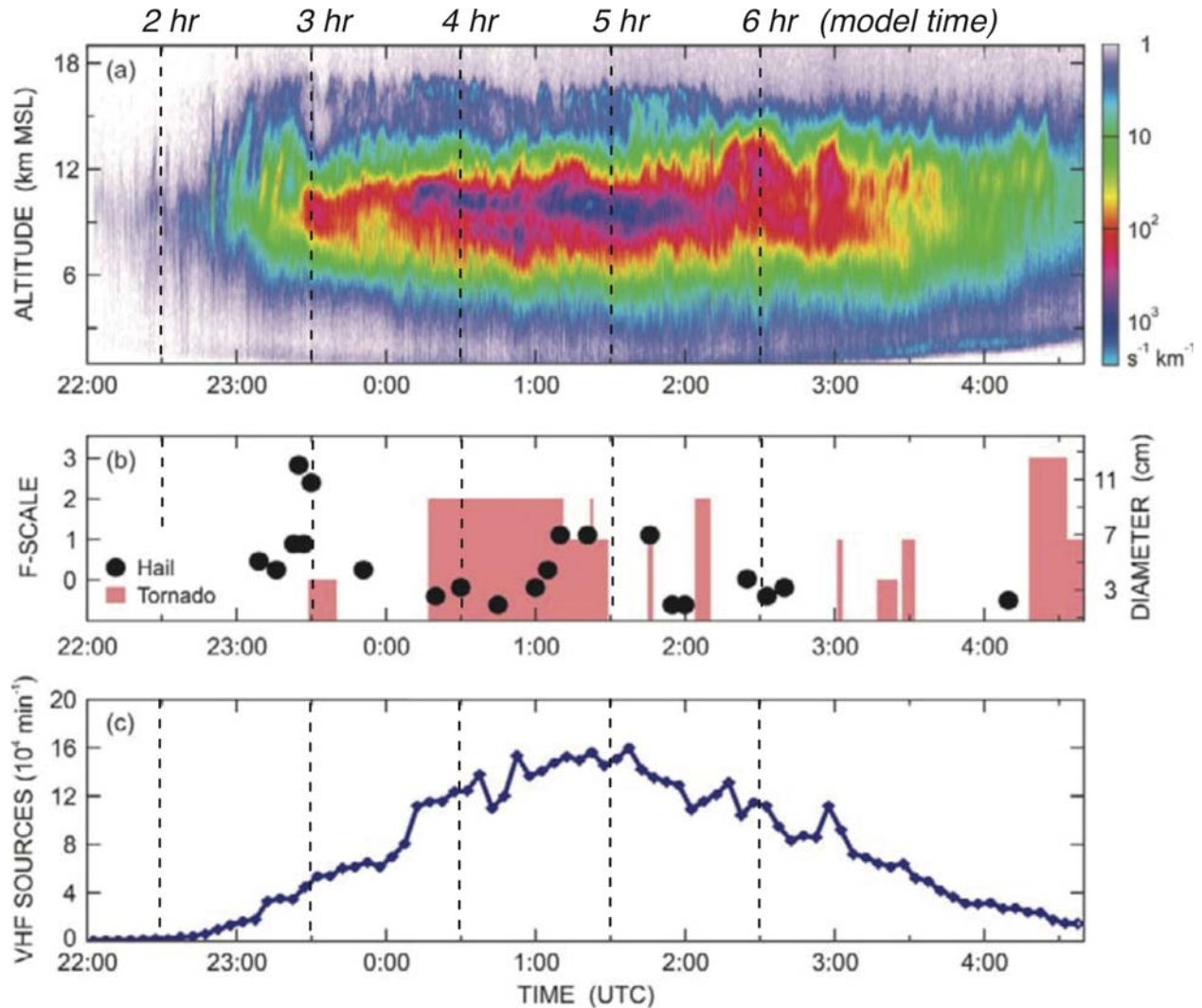


Figure 1. Temporal evolutions of VHF source detection profiles from the OK-LMA, hail and tornadoes, and total VHF sources in the 29-30 May 2004 Geary supercell storm (adapted from MacGorman et al. 2008). (a) time-height source density profiles. (b) reported time and F-scale tornadic damage rating and reported time and diameter of large hail. (c) 5-min average of the number of mapped VHF sources per minute. Panels (a) and (c) illustrate the LMA's decreasing source detection efficiency with increasing storm range from the LMA network before 0000 UTC (storm approaching from west) and after 0230 UTC (storm receding to east). Vertical dashed lines denote equivalent model-simulation time (hours) as listed in Table 1.

2. OBSERVED STORM HISTORY

The first identifiable cumulus towers and initial radar echo of the Geary supercell storm occurred just east of the dryline in southwest Oklahoma, U.S.A. at roughly 2030 UTC (all times are Universal Time) on 29 May 2004 (e.g., Calhoun et al., 2013; see also Fig. 1 and Table 1). The estimated initial convection has been reliably located and timed by examining sequences of radar, visible satellite, and LMA plots (not shown). The initial organized storm object associated with the convection initiation (CI) event formed within 30-45 min after initial cloud development. The Geary storm formed in a convectively unstable, horizontally rather homogeneous boundary layer (BL) east of the dryline. The storm subsequently entered and evolved within an increasingly cooler, moister, and more stable BL characterized by a 3 °C decrease of surface potential temperature as it moved away from the dryline. Over the next two hours it

Table 1. Timing of key events during the observed and simulated Geary, Oklahoma storms on 29-30 May 2004. Acronyms in the table include the following: "LP" = "low-precipitation"; "CL" = "classic"; "EnKF" = "ensemble Kalman filter"; "EFM" = balloon-borne "electric field meter"; "DD" = "dual-Doppler"; "BWLR" = "bounded weak lightning region"; "LLM" = "low-level mesocyclone"; "HP" = "high-precipitation". Cited papers are Calhoun et al. (2013), or "C13"; and Calhoun et al. (2014) or "C14".

Time (UTC)	Model time (hour/min)	Observed/modeled storm events
2030	0	model initialization
2130	1	multicell storm
2230	2	storm begins right-turn, LP supercell
2330	3	storm ends right-turn, CL supercell, LLM
2335	3 hours 5 minutes	converged EnKF started (C14)
2346	3 hours 16 minutes	EFM launch into Geary storm
2347	3 hours 17 minutes	first DD analysis (C13)
2355	3 hours 25 minutes	BWLR (C13)
0016	3 hours 46 minutes	BWLR, strong LLM (C13)
0027	3 hours 57 minutes	BWLR (C13)
0030	4	HP supercell
0031	4 hours 1 minute	EFM at max altitude in storm
0050	4 hours 20 minutes	BWLR in EnKF (C14)
0052	4 hours 22 minutes	last DD analysis (C13)
0055	4 hours 25 minutes	EnKF ended (C14)
0130	5	intense LLM, storm reorganizes
0230	6 hour	HP supercell, simulation ends

moved northeastward and intensified, then entered the cooler and more moist BL as it turned eastward by 2330 (e.g., Table 1). The storm produced several tornadoes (included two rated at F-2 intensity) as well as copious total lightning and predominantly negative cloud-to-ground (-CG) flashes (e.g., Fig. 9 of Calhoun et al. 2013). The storm also produced several positive cloud-to-ground (+CG) flashes. The CG flash rates were typically on order of 10-20 min^{-1} , but were occasionally as low as order 1 min^{-1} . Although total flash rates were typically on the order of 300 min^{-1} , total flash rates were occasionally as high as 500 min^{-1} . The storm subsequently turned to an east-northeast heading, initiated a transient multicellular reorganization phase by around 0130, and ultimately reorganized as an HP supercell after 0230 on 30 May. The storm persisted until around 0500 when it underwent a rapid final decay. The present study emphasizes the storm's electrical evolution in relation to its dynamics and microphysics during the first 6 hours of its lifetime (2030 on 29 May to 0230 on 30 May 2004).

3. CLOUD MODEL

3.1. Model description

The NSSL three-dimensional cloud model (COMMAS) employs non-hydrostatic and fully compressible airflow dynamics, including prognostic equations for the three momentum components and pressure, potential temperature, and turbulent kinetic energy (Mansell et al. 2010). The model also includes parameterized 2- and 3-moment cloud microphysics and additional conservation equations for the mixing ratios of water vapor and hydrometeors (e.g., Mansell et al. 2010, Mansell and Ziegler 2013).

Storm electrification is treated in the model via a range of parameterized ion and hydrometeor charging processes (e.g., Mansell et al., 2005, Mansell et al. 2010) and the discrete breakdown model

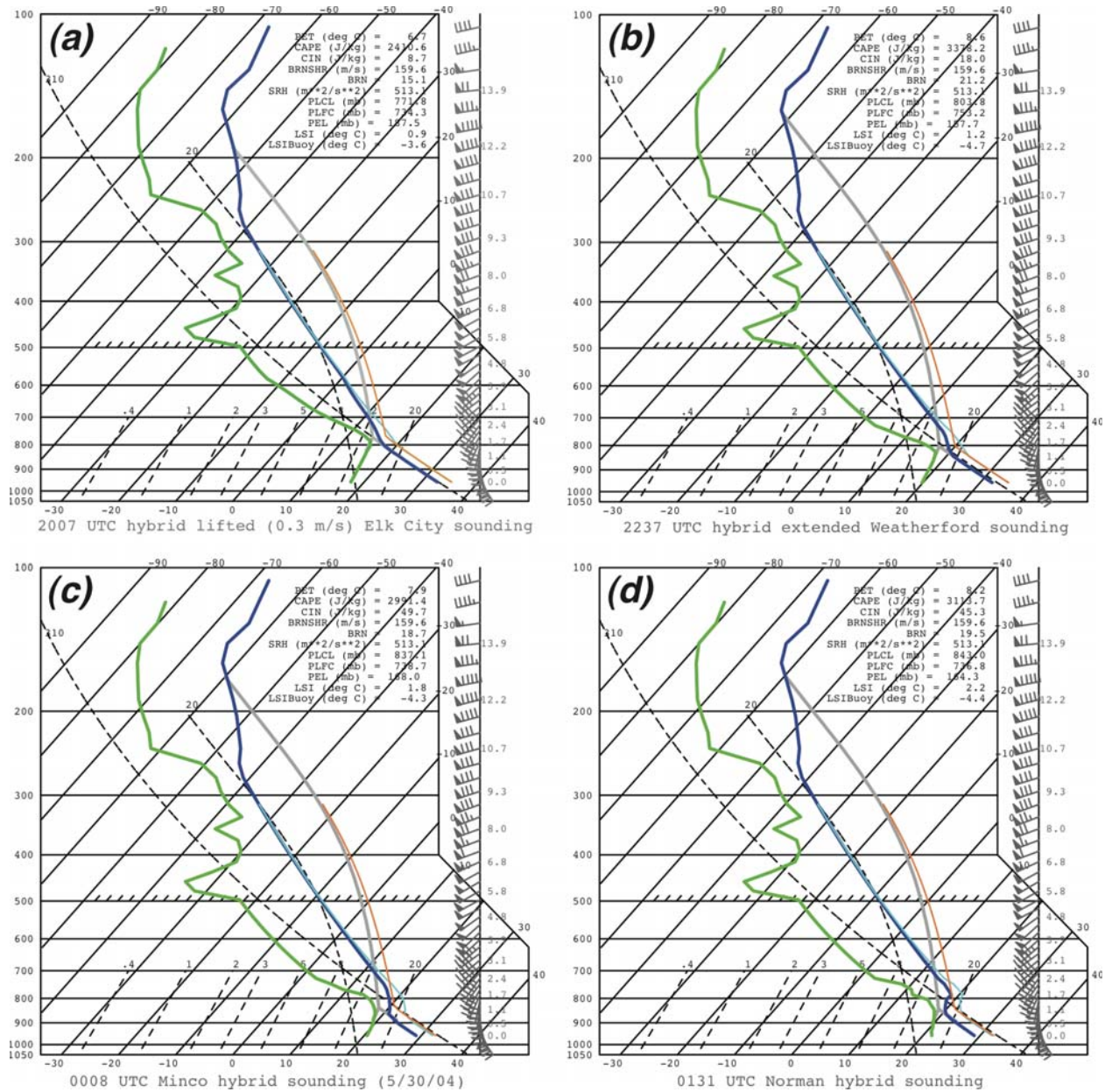


Figure 2. Soundings in the environment of the 29-30 May 2004 Geary supercell storm. The soundings are arranged from west to east and with increasing time as the mobile sounding system follows the moving Geary storm: (a) westernmost sounding (Elk City OK at 2000 UTC); (b) first sounding to east on edge of moister, cooler boundary layer (Elk City at 2200 UTC 29 May); (c) second sounding to east in much moister, cooler boundary layer (Minco, OK at 0006 UTC); (d) easternmost sounding in moist, cool boundary layer (Norman, OK at 0130 UTC 30 May).

(DBM) parameterization of individual branched lightning flashes (Mansell et al., 2002). The model also solves conservation equations for positive and negative fast ion and hydrometeor space charge densities. Since as previously noted the Geary storm produced predominantly negative ground flashes, the storm was inferred to be dominated by a substantial main negative charge region (possibly within a normal-polarity tripolar or quadrupolar charge structure). The present storm simulation employs the Saunders

and Peck (SP98) noninductive charging scheme (as implemented by e.g., Mansell et al., 2005), since the SP98 parameterization has commonly produced a normal tripolar charge arrangement in previous storm simulations. Other charging mechanisms (e.g., strong inductive graupel-ice charging) are very similar to previous model configurations (e.g., Mansell et al., 2005).

3.2. Model initialization, lateral boundary conditions, and integration

An option for time-dependent, one-way lateral inflow boundary conditions for the moving storm-relative domain has been added to the COMMAS model, allowing the simulated storm to experience observed variable ambient conditions as it evolves and moves through mesoscale temperature and moisture gradients. The Geary storm simulation is initialized in an idealized horizontally heterogeneous environment derived from four input soundings (Fig. 2). The soundings of the Geary storm's inflow environment were obtained in a storm-following reference frame by coauthors Ziegler and Mansell during the TELEX field program (MacGorman et al. 2008). The soundings were obtained by initially deploying to the area of anticipated CI, obtaining an initial sounding of the CI environment, and subsequently tracking the storm-relative inflow location while releasing soundings at approximately a 1.5 - 2 hour interval. Soundings were obtained at Elk City (2000 on 29 May), Elk City (2200), Minco (0006 on 30 May), and Norman (0130).

All model soundings have been assigned a representative wind profile based on the 0006 Minco sounding. The hodograph is characterized by strong directional turning and speed shear in the lowest 3 km and a storm-relative helicity of $513 \text{ m}^2 \text{ s}^{-2}$ at the nominal observed and simulated mature storm motion averaging from 270 deg at 9 m s^{-1} during the severe right-moving storm phase. An additional model option to introduce a time-varying observed wind profile is under development, and will be reported in future studies. The mid-tropospheric (MT) temperature and humidity profiles were uniformly smoothed to increase static stability and eliminate local neutrally-stable layers (thought to be related to highly transient internal gravity waves that are not representative of the broader mesoscale MT environment).

The western sounding (sounding 1, Fig. 2a), assumed to be the model base state following the method described by Ziegler et al. (2010), has 2410 J kg^{-1} of virtual-temperature-based mixed layer convective available potential energy (MLCAPE). The first sounding to the east of the westernmost sounding has an MLCAPE of 3378 J kg^{-1} (sounding 2, Fig. 2b). The unstable western sounding has about 9 J kg^{-1} of virtual-temperature-based mixed-layer convective inhibition (MLCIN), while sounding 2 has an MLCIN of 18 J kg^{-1} . The surface potential temperatures of soundings 2-4 are respectively 0.69 C , 3.52 C , and 3.88 C colder than the surface potential temperature of the base-state sounding 1, and the cooler BLs are also progressively more moist. The combined MLCAPE and helicity values support an intense supercell storm with a strong low-level mesocyclone (LLM).

The temperature and vapor mixing ratio fields are analytically prescribed within a large, fixed mesoscale grid domain. The smaller, moving storm simulation domain is nested inside the mesoscale domain and derives its initial and time-dependent inflow lateral boundary conditions from the parent mesoscale domain following the method described by Ziegler et al. (2010). To approximately match a possible existing surface mesoanalysis of the storm's environment, the isentropes and isohumes could optionally be assigned a best-fit, user-input rotation angle with respect to due north. However, best results were obtained by applying the alternate user-input rotation angle option, according to which isolines at each level are rotated to be parallel with the winds at that level (Ziegler et al. 2010). The temperature and vapor mixing ratio fields are horizontally homogeneous in the western and eastern ends of the mesoscale domain according to the first (Fig. 2a) and fourth (Fig. 2d) soundings, respectively, and vary piecewise-linearly between soundings 2-3 (Fig. 2b-c) and soundings 3-4 (Fig. 2c-d). The winds in the mesoscale domain are horizontally homogeneous based on the fixed input wind profile.

The 6-hour storm simulation is performed within a storm-following 160 km (east-west) x 160 km (north-south) x 23.8 km (height AGL) domain. The model domain employs a constant horizontal grid spacing of 1 km and a vertically stretched grid from a 100 m vertical spacing at the ground to 500 m aloft. Vertical motion is initiated by imposing a weak Newtonian forcing or nudging in the vertical momentum equation within a cylindrical, cloud-following volume that is 8 km in radius through the lowest 3.6 km

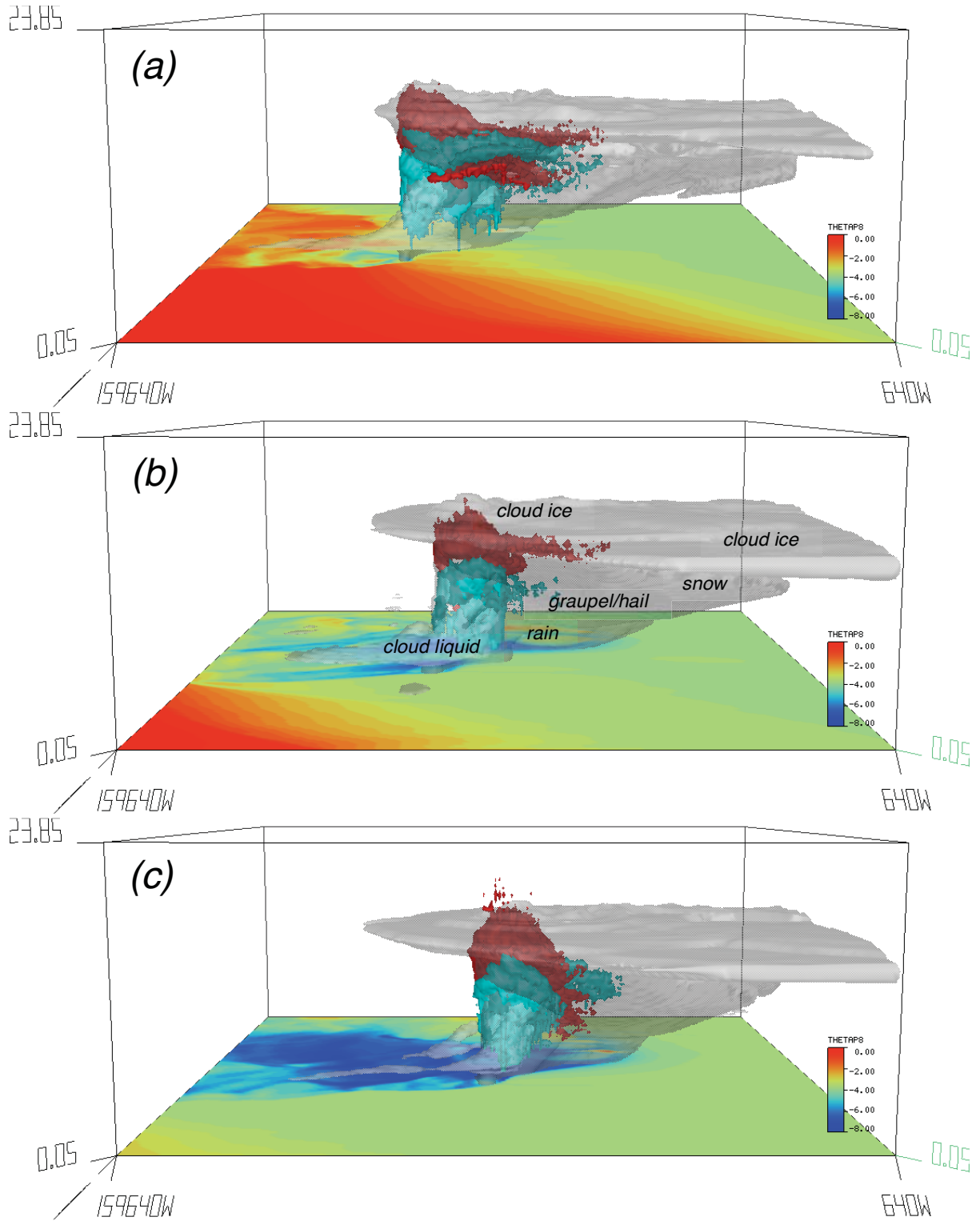


Figure 3. 3D views of the simulated supercell storm looking north at (a) 3 hours, (b) 4 hours, and (c) 5 hours of integration. Red surfaces enclose the previous 10-min period of integrated positive flash leader densities, while light blue surfaces enclose negative flash densities. The light gray surface encloses the combined liquid and ice cloud volumes, while the dark gray surface encloses the combined rain, graupel, hail, and snow precipitation volumes. The color-filled horizontal surface denotes the perturbation potential temperature from the base state value at the lowest model level (50 m AGL).

AGL. The Newtonian nudging forcing is maintained for the first 40 min of integration, then deactivated as the simulated storm initiates a precipitation-induced cold pool to maintain its own dynamically-forced BL lifting (i.e., simulated CI). The dynamic time step for the model's forward integration is 4 seconds.

4. RESULTS AND DISCUSSION

4.1. Overall evolution and morphology of the simulated storm

The observed and simulated storms initiate and move northeastward during the first hour as a strong multicell storm (Table 1). The observed and simulated storms subsequently evolve into a “low-precipitation” or “LP” supercell and initiate a gradual right-turn by two hours, and finally complete the right turn after three hours as an eastward-moving “Classic” (CL) supercell containing an intensifying low-level mesocyclone or LLM (e.g., Fig. 3a). The eastward-moving observed and simulated storms gradually evolve toward a “High-precipitation” (HP) supercell by 4 hours (e.g., Fig. 3b), and as reported by Calhoun et al. (2013) also develop transient BWLRs and undergo further intensification of the LLM. The observed and simulated storms maintain an HP supercellular structure through 5 hours (Table 1, Fig. 3c), by which time a separate EnKF analysis of the storm's electrification (Calhoun et al. 2014, see Table 1) produced a subsequent (numerically-simulated) BWLR. The observed storm and the modeled storm in the present study turn slightly left toward an east-northeast heading during the storm's reorganizing phase after 5 hours (Table 1).

The simulated storm in the present study develops several features typical of observed supercells. Among these features (not shown) are: (1) a persistent and intense, rotating mesocyclonic updraft; (2) a hook echo and BWER associated with the rotating updraft; (3) hail both at the surface and aloft (as simulated using the new 3-moment bulk hail microphysics scheme referred to in section 3.1; see also discussion in section 4.3). A strong LLM (suggestive of the role of storm-induced baroclinic horizontal vorticity generation and subsequent tilting into the vertical) steadily intensifies during the CL-HP phases of the observed and simulated Geary supercells, with the simulated LLM attaining vertical vorticity from $\sim 20 \times 10^{-3} \text{ s}^{-1}$ around 3 hours up to as large as $100 \times 10^{-3} \text{ s}^{-1}$ around 5 hours. The simulated supercell at 5 hours (e.g., Fig. 3c) broadly corresponds to radar-observed morphology at the equivalent observed times (Table 1 and e.g., Calhoun et al. 2013).

The simulated storm intensity as inferred from peak reflectivity (Fig. 4a), updraft mass flux (Fig. 4b), and total precipitation mass (Fig. 4c) increases in stages during the first 3 hours owing to the storm's eastward movement into the progressively more moist BL (containing larger values of MLCAPE) combined with the storm's right-turn which increases low-level convergence between 2 and 3 hours.

The cloud base height is uniform before 2 hours, after which time the storm enters the moist, cool BL and the cloud base subsequently decreases due to a lowering lifting condensation level (LCL). Lower LCL height is a known predictor favoring increasing supercell tornado probability, and the strongest observed tornadoes occurred during this time period of decreasing simulated LCL height. On the other hand, increasing BL coldness and the increasing inversion strength (Fig. 2b-d) tends to offset the storm's cold pool intensity. As a result of decreasing cold pool temperature deficit, the decreasing lifting intensity at the outflow boundary reduces the vertical flux of inflow air toward its level of free convection or LFC (Ziegler et al. 2010). The net effect of the combined lower LCL and the limited cold pool temperature contrast is the attainment of an overall maximum storm intensity by about 3-4 hours (consistent with findings of Ziegler et al. 2010), with a subsequent slight overall decrease in intensity between 4 and 6 hours (Fig. 4).

The increasing peak reflectivity after 3 hours delineates the transition from the CL to HP storm phases, with extreme peak reflectivities exceeding 70 dBZ indicating presence of increasing mass and mean size of modeled hail (see related discussion in sections 4.2-4.3). Given modest decreases of the main updraft intensity after 4 hours, it is speculated that the slight decreasing trend of total precipitation mass is related mainly to increasing precipitation fallout owing to larger graupel and hail particle contents (e.g., discussion in section 4.3), sizes, and corresponding fallspeeds.

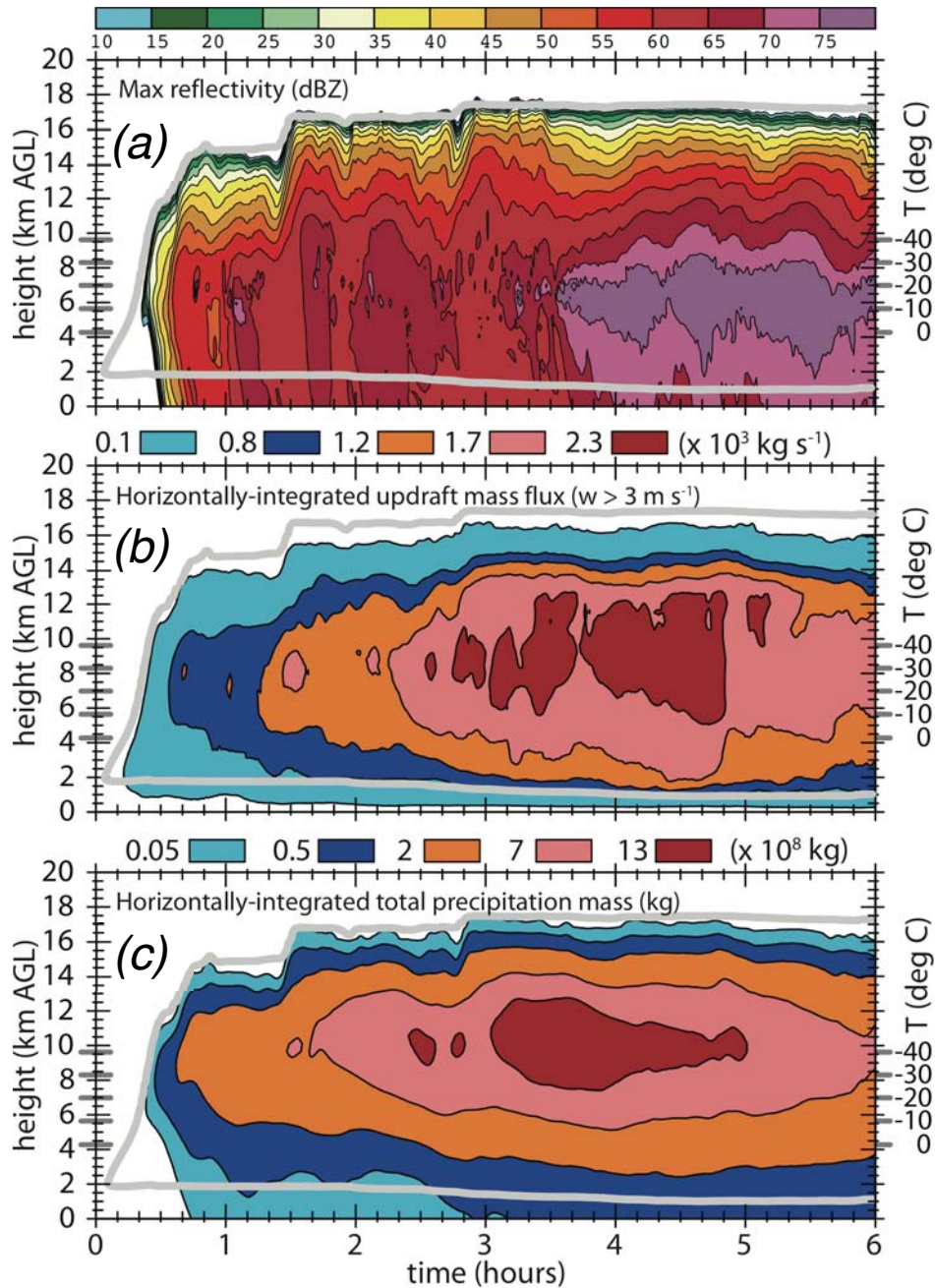


Figure 4. Time-height profiles of (a) maximum reflectivity (dBZ), (b) the horizontally-integrated updraft mass flux within the volume containing $w > 3 \text{ m s}^{-1}$, and (c) the horizontally-integrated total precipitation mass (rain, snow, graupel, hail) in the simulated supercell storm. Color fill levels are indicated by the keys above each panel. The thick gray contour denotes the lower and upper cloud (water + ice) boundary. The labeled axis at the right side of each panel denotes the base-state temperature (C) profile.

4.2. Relation between simulated kinematics, precipitation, and lightning

A combination of noninductive and inductive charging, ion and lightning-induced charging, and 3-D charge transport associated with airflow and differential fallspeeds produce a complex, predominantly tripolar or quadrupolar charge arrangement in the main supercell updraft region of the simulated storm.

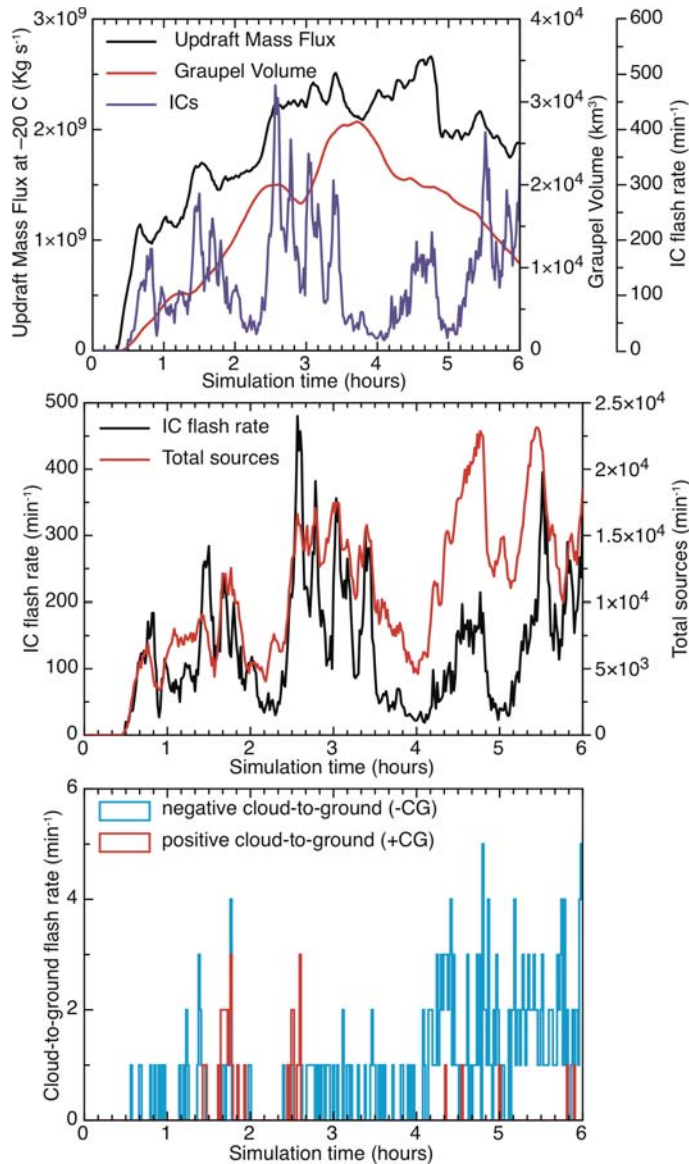


Figure 5. Time evolution of domain-integrated kinematic, microphysical, and lightning quantities in the simulated storm. (a) updraft mass flux at -20 C, graupel volume, and intra-cloud (IC) flash rate; (b) IC flash rate and total sources (DBM flash segments); (c) positive and negative cloud-to-ground (+CG and -CG) flash rates.

microphysical charge separation rate within the storm core. Note that the number of total sources (i.e., as estimated from total DBM flash segments) has a pronounced upward trend despite transient total lightning minima at 2, 4, and 5 hours (Fig. 5b). The latter increase of total flash segments in turn implies that individual simulated flashes are becoming progressively more extensive as the storm's net charge reservoir expands with time.

Broad regions of either positive or negative net space charge may be inferred from regions containing DBM flash segments of predominantly negative or positive charge, respectively (Fig. 6). Lightning channel charges in the simulated supercell storm display a normal-polarity tripole prior to 1 hour (Fig. 6). The overall storm net charge structure after 1 hour is characterized by a quadrupole combining the earlier normal-polarity tripole with an upper-level negative charge region (Fig. 6). These results are broadly

After developing the first intracloud (IC) flash at around 30 minutes of simulated storm evolution (i.e., 2100, Figs. 5a-b, see also Table 1), the simulated storm subsequently develops sustained periods of IC flash rates of 100-200 min^{-1} and peak IC flash rates of up to 400-500 min^{-1} (Figs. 5a-b). After developing the first negative cloud-to-ground (-CG) flash at 34 min (Fig. 5c), the simulated storm subsequently develops CG flashes of both polarities at rates of up to 4-5 min^{-1} . Four strong peaks in IC flash rates at 1.5, 3, 4.5, and 5.5 hours reveal a highly transient behavior of the simulated total lightning activity, with the (significantly lower) CG rates roughly in phase or slightly lagging the periodicity of the IC flash rates (e.g., as in Ziegler and MacGorman 1994). Strong peak vertical electric fields in excess of 200 kV m^{-1} (not shown) develop rapidly due mainly to cloud ice and graupel initiation, growth, and large rebounding collision rates in the supercooled, cloudy updraft (e.g., Ziegler et al. 1991, Ziegler and MacGorman 1994). This strongly electrified state persists through the simulated storm's 6-hour evolution due to the maintenance of the intense, mixed-phase supercellular deep-convective updrafts.

Visually strong correlations are suggested between the detrended time series of updraft mass flux or graupel volume and IC flash rate (e.g., as previously shown by Kuhlman et al. 2006). However, the occurrence of pronounced transient absolute IC flash rate minima may imply that local transient decreases of mixed-phase ice and graupel contents in the intense updraft are driving corresponding transient reductions of the

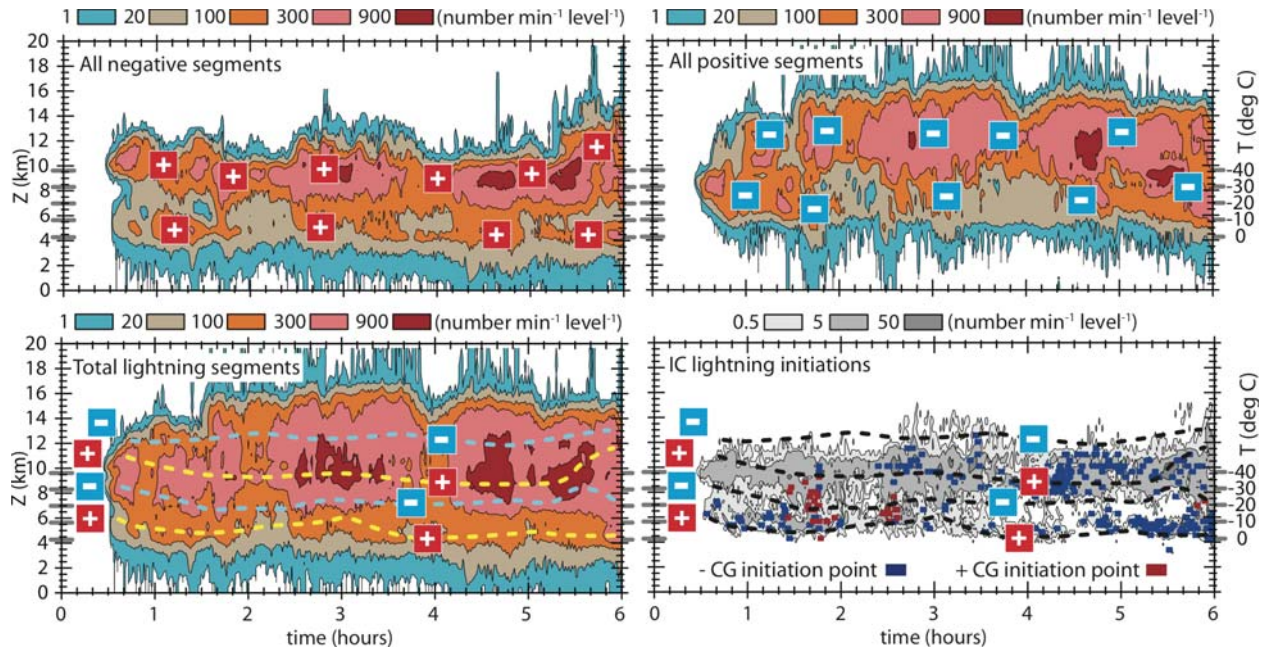


Figure 6. Total lightning leader and flash initiation quantities in the simulated 29-30 May 2004 Geary supercell storm. Lightning initiations and leader quantities are 1-min, horizontally integrated totals at each level and each 1-min interval output time. (a) Total negative flash segments (i.e., most closely related to LMA negative breakdown source densities), with plus symbols locating estimated ambient positive net space charges; (b) total positive flash segments, with minus symbols locating estimated ambient negative net space charges; (c) total positive and negative flash segments; (d) total intra-cloud (IC) initiations (gray fill) and initiation points of cloud-to-ground (CG) flashes lowering negative and positive charge to ground (blue and red boxes, respectively). Yellow and blue dash curves in panel (c) trace approximate layers of positive and negative net charge (respectively) as inferred from negative and positive flash segments in panels (a) and (b) respectively. The dashed curves in panel (d) are as in panel (c), but are black-filled for clarity.

consistent with SP98 storm simulations of Mansell et al. (2005) and Kuhlman et al. (2006). The simulated total negative cloud-to-ground (–CG) initiations account for roughly 40% of the simulated total flash initiations in the layer from -5°C to -15°C . The four predominant flash types in the simulation (i.e., as aggregated in Fig. 6 with initiation locations in Fig. 6d) are as follows: (1) ICs initiated at upper levels with positive-above-negative leaders (i.e., “+/-” polarity); (2) ICs initiated at middle levels with “+/-” polarity; (3) –CG discharges (“+/-” polarity) initiated at middle and upper levels; and (4) +CG discharges (“-/+” polarity) initiated at middle levels. The leader branches and initiation points of simulated IC and CG flashes (Fig. 6a-c and Fig. 6d respectively) are concentrated in or near the mixed-phase convective updraft region and its associated main precipitation core in radar reflectivities ranging from 35 to 75 dBZ (Fig. 4a vs. Fig. 6).

4.3. Bounded weak lightning regions (BLWRs)

The simulated supercell storm contains transient “bounded weak lightning regions” or BWLRs (i.e., analogous to the lightning-weak “holes”) in and near the main updraft and BWER, consistent with radar and LMA observations and recent Ensemble Kalman Filter (EnKF) analyses of the Geary storm (Fig. 7). The vertically-integrated negative leader composite (i.e., color-filled field in Fig. 7) serves as an effective proxy for observed LMA sources which are dominated by negative breakdown. A pronounced, completely enclosed modeled BWLR is present at 2 hours (Fig. 7a) and 3 hours (Fig. 7b). The modeled BWLR at 4 hours has decreased in areal extent and moved toward the northwest side of the main supercell updraft (Fig. 7c), while the former BWLR has filled by 5 hours (Fig. 7d).

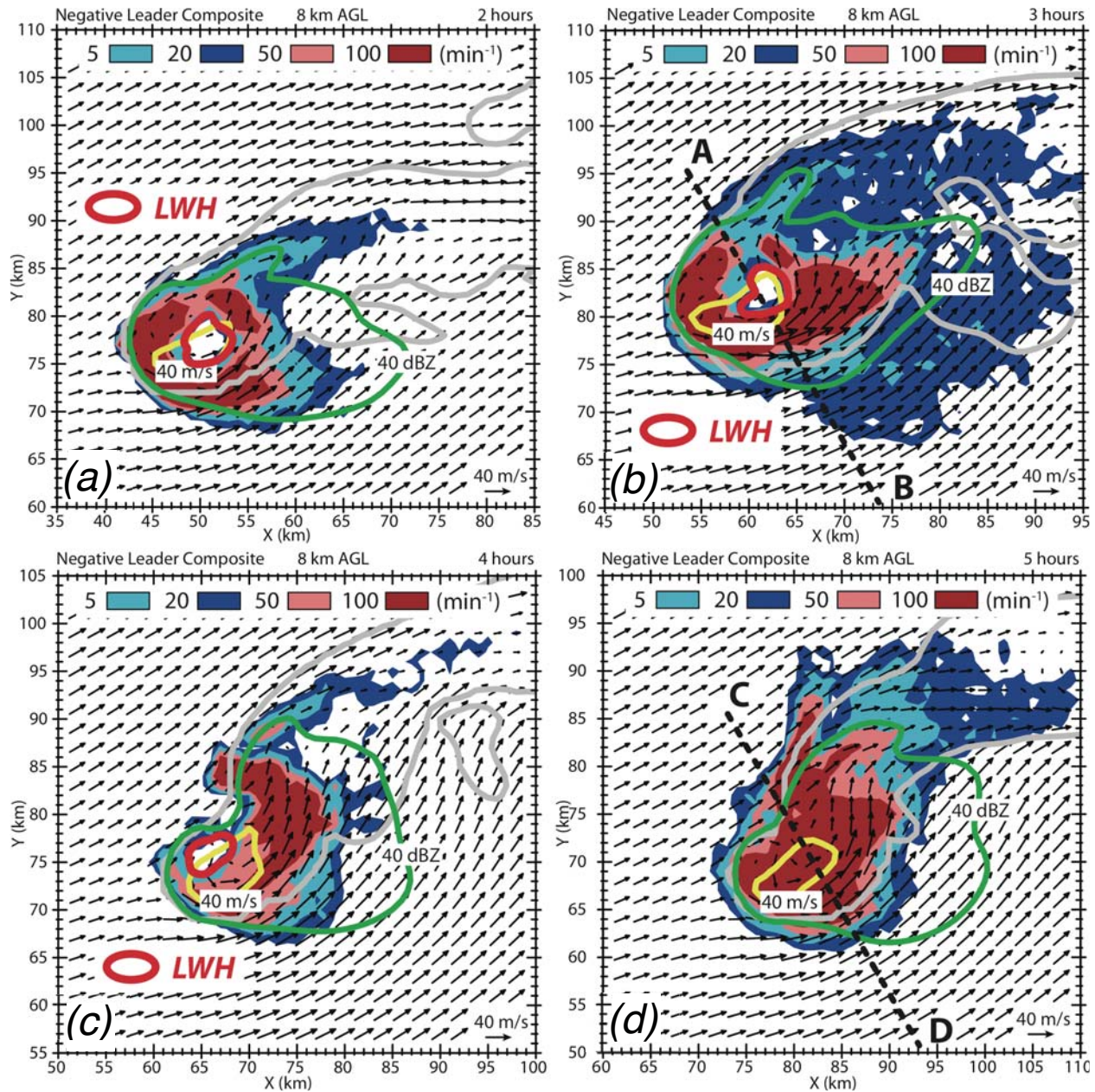


Figure 7. Horizontal "LMA plots" of vertically-summed negative flash densities in the simulated 29-30 May 2004 Geary supercell storm. (a) 2 hours; (b) 3 hours; (c) 4 hours; (d) 5 hours. Note "lightning weak holes" (LWH) or "bounded weak lightning regions" (BWL) at hours 2-4. The 40 m s^{-1} updraft core (yellow curve), 40 dBZ reflectivity (green curve), and combined cloud water/ice outline (gray curve) at 8 km AGL are overlaid.

The latter sequence of BWER evolution associates with intensification of the low-level mesocyclone (LLM) which increasingly injects graupel-meltwater rain via the radar "hook-echo" into the base of the main updraft (e.g., Fig. 8). The in-filling of the mid-level main updraft and former BWER with graupel (Fig. 8, top row) and hail (Fig. 8, second row) accompanies the storm's progression from the CL to HP supercell stages (e.g., note lowering of base of precipitation region at 5 hours relative to the former BWER at 3 hours). Graupel and hail fallout through the melting level on the sloping updraft flanks leads to a updraft reinjection-recycling process characterized by a sequence of meltwater rain generation and vertical rainwater advection on the main updraft flanks (not shown), culminated by midlevel freezing to

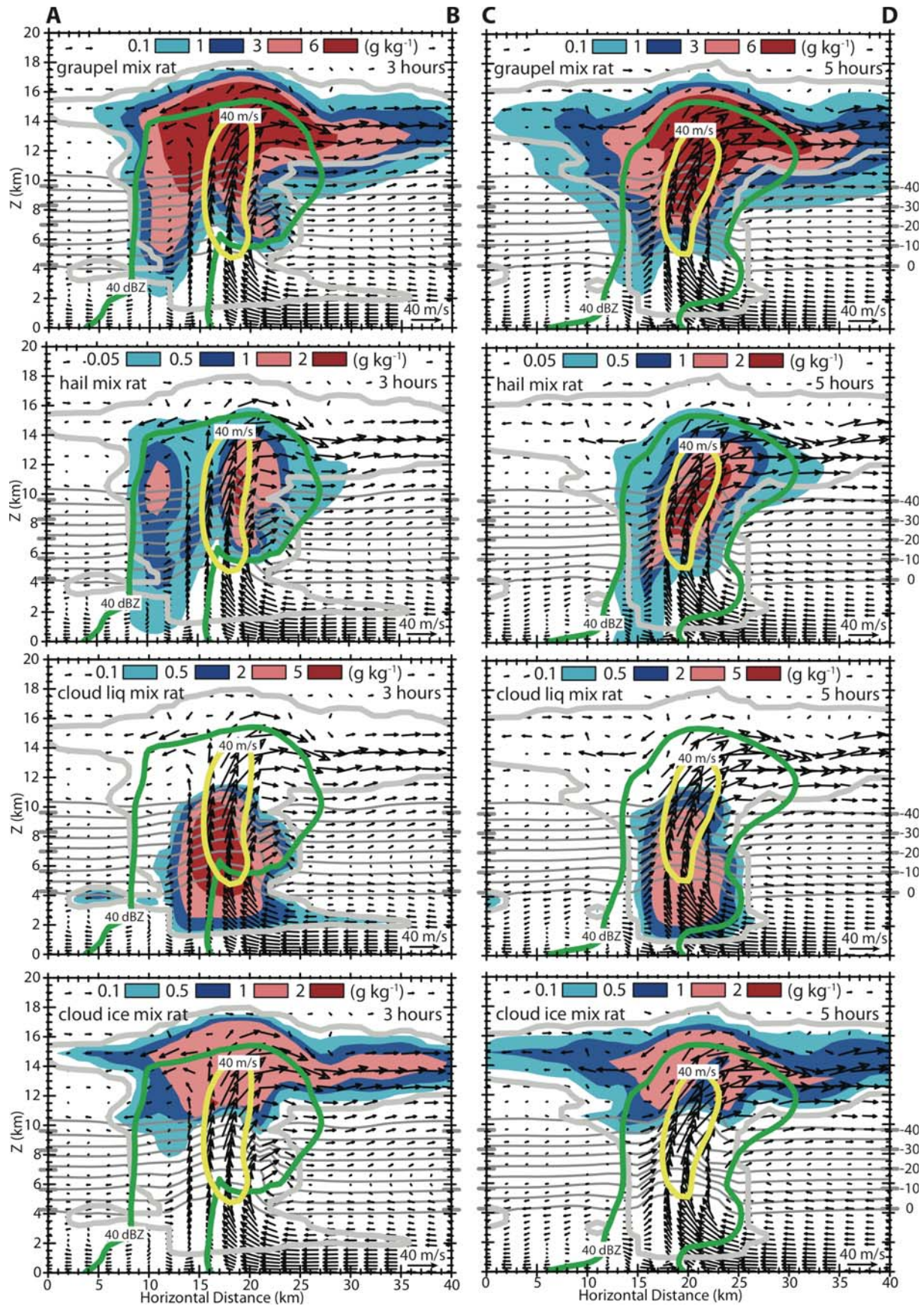


Figure 8 (continued from previous page). Vertical cross-sections of precipitation, cloud, and airflow in the simulated 29-30 May 2004 Geary supercell storm. (left column) 3 hours; (right column) 5 hours. Top row to bottom row: graupel mixing ratio (g kg^{-1}); hail mixing ratio (g kg^{-1}); cloud liquid mixing ratio (g kg^{-1}); cloud ice mixing ratio (g kg^{-1}). Note locations of cross-section A-B and C-D in Fig. 7b and 7d respectively. The 40 m s^{-1} updraft core (yellow curve), 40 dBZ reflectivity (green curve), combined cloud water/ice outline (light gray curve), and isotherms at a 5 C interval (dark gray curves) in the cross-section are overlaid.

form riming graupel (Fig. 8, top row) and large hail (Fig. 8, second row). In other words, the ultimate source of increasing graupel and hail mixing ratios at the summit of the lowering BWER in the main updraft is meltwater rain drop freezing following by riming grow and conversion to hail. The increased riming growth of graupel and hail in turn increasingly depletes cloud liquid water (Fig. 8, third row) and also reduces cloud ice in the anvil which is primarily forced by cloud water vertical advection and freezing around -40 C (Fig. 8, bottom row).

The stimulation of precipitation growth in the mixed-phase updraft subsequently initiates intense noninductive graupel-ice charging in the updraft core. The potential main noninductive charging zone from 0 to -40 C in the cloudy main updraft is largely free of any space charges (thus free of lightning flashes) at 3 hours (Fig. 9, left column), but has filled with space charge by 5 hours (Fig. 9, right column). Thus as the simulated mixed-phase BWER subsequently fills with charging graupel, new charge centers form in the midlevel updraft that subsequently supports both lightning flash initiation and leader propagation through the new charge center (Fig. 9). Space charge on graupel (Fig. 9, top row) and hail (Fig. 9, second row) increasingly form midlevel positive centers on the south flank of the strong updraft in high supercooled cloud liquid water contents (Fig. 8). Conversely on the northern storm flank which contains weaker updrafts and lower values of supercooled cloud liquid water (Fig. 8), the SP98 noninductive charging results in a charging sign reversal with negative charge to graupel and hail (Fig. 9, top and second rows respectively). Since cloud ice attains opposite charge from riming graupel and hail, the resulting cloud ice space charges have a complex 3-D structure (Fig. 9, third row). The horizontal variation of noninductive charging sign in turn results in the approximately quadrupolar 3-D net space charge structure due to the subsequent 3-D transport of all space charges combined with lightning-induced charges (Fig. 9, bottom row).

5. CONCLUSIONS

This study has successfully simulated the dynamical, microphysical, and electrical evolution of the Geary supercell through the first 6 hours of its lifecycle. A realistic prescription of the storm's horizontally heterogeneous mesoscale environment via initial and time-dependent lateral inflow boundary conditions has suppressed the development of secondary convection, thus maintaining the storm's observed isolated character while also realistically modulating its intensity and mode. The main objective of the study has been to reproduce the Geary storm's observed transient "lightning-weak holes" or LWHs, which (for improved consistency with the conventional radar-based terminology "BWER") the study refers to as "bounded weak lightning regions" or BWLRs. The simulation has successfully produced modeled BWLRs that bear considerable resemblance to the observed BWLRs.

The study has successfully verified the hypothesis that the modeled BWLR is associated with regions of the supercell storm that contain weak hydrometeor and net space charges, including BWERs but also regions containing cloud and precipitation particles that experience little or no charging along their trajectories. The study has also validated the corollary hypothesis that graupel- and hail-meltwater are entrained into the sloping flanks of the main updraft via the storm's developing radar "hook-echo" and mesocyclone, thus stimulating vertical meltwater advection and drop freezing to initiate riming graupel and subsequent conversion to hail. It has been demonstrated that the graupel and hail invigoration via drop recycling-freezing leads to redevelopment of riming, noninductively charged graupel and hail within the in-filled BWER, thus generating new net charge centers and ultimately stimulating lightning activity within the main updraft where a BWLR formerly existed. The simulated supercell storm is shown to weaken after penetrating into the homogeneous stable BL between ~ 3 -5 hours, subsequently evolving

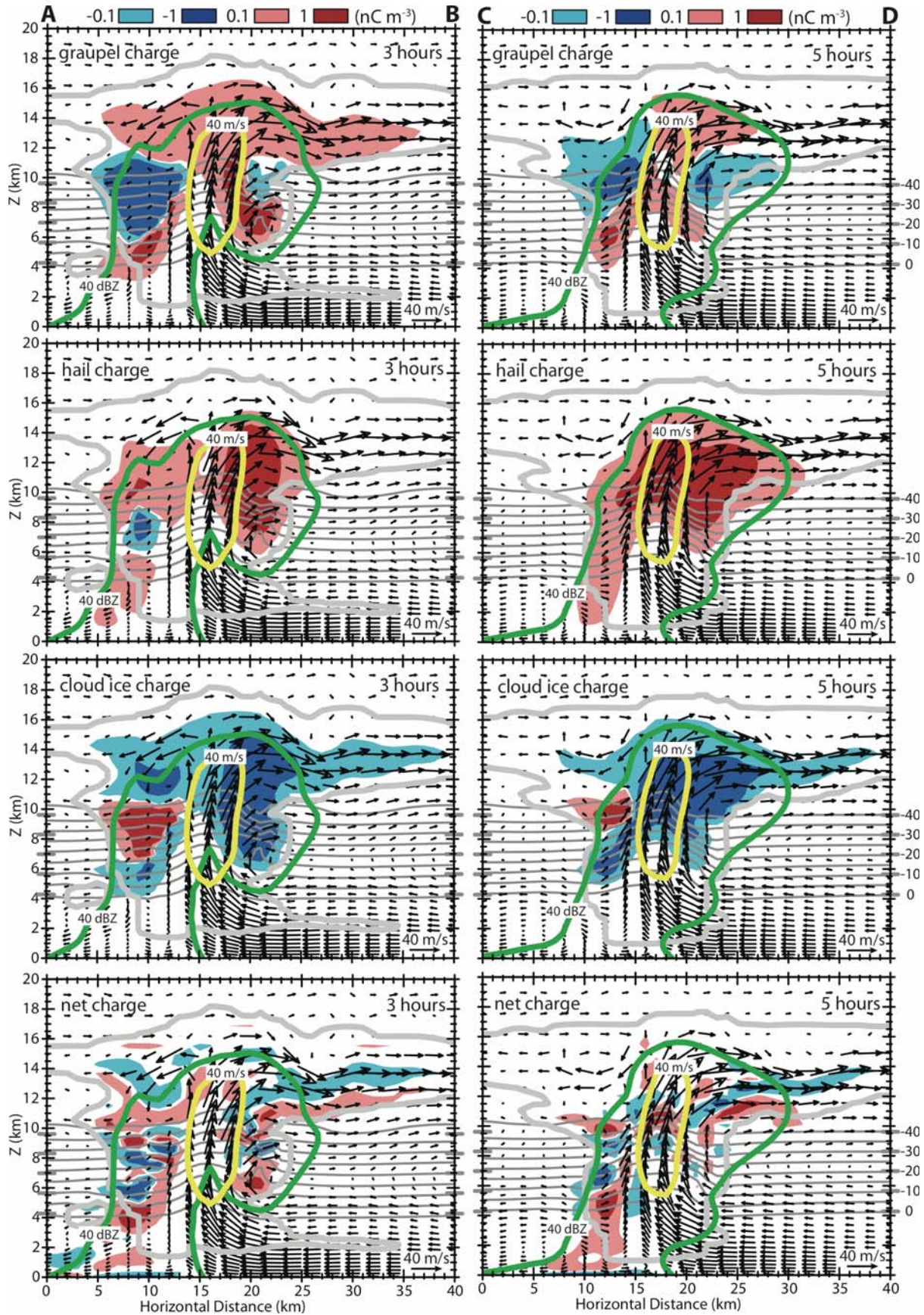


Figure 9 (continued from previous page). Vertical cross-sections of space charge and airflow in the simulated 29-30 May 2004 Geary supercell storm. (left column) 3 hours; (right column) 5 hours. Top row to bottom row: graupel space charge (nC m^{-3}); hail space charge (nC m^{-3}); cloud ice space charge (nC m^{-3}); net space charge (nC m^{-3}). Note locations of cross-section A-B and C-D in Fig. 7b and 7d respectively. The 40 m s^{-1} updraft core (yellow curve), 40 dBZ reflectivity (green curve), combined cloud water/ice outline (light gray curve), and isotherms at a 5 C interval (dark gray curves) in the cross-section are overlaid.

into a transient strong multicellular storm mode with decreasing magnitudes of updraft, precipitation content, electrification, and flash rate. Similar results were previously obtained from modeling studies of kinematics, dynamics, microphysics, and electrification in the 22 May 1981 Binger, Oklahoma supercell storm (Ziegler and MacGorman 1994, Ziegler et al. 2007, Ziegler et al. 2010).

ACKNOWLEDGEMENTS: This study was supported by NSSL, the Cooperative Institute for Mesoscale Meteorological Studies of the University of Oklahoma, and by NSF grants ATM-0451639 and ATM-1063966. Resources for our TELEX mobile storm environmental soundings were provided by a grant from the NOAA/OAR/United States Weather Research Program (USWRP).

REFERENCES

- Calhoun, K., D. MacGorman, C. Ziegler, and M. Biggerstaff, 2013: Evolution of lightning activity and storm charge relative to dual-Doppler analysis of a high-precipitation supercell storm. *Mon. Wea. Rev.*, 141, 2199-2223.
- Calhoun, K., E. Mansell, D. MacGorman, and D. Dowell, 2014: Numerical simulations of lightning and storm charge of the 29-30 May 2004 Geary, Oklahoma supercell thunderstorm using EnKF mobile radar data assimilation. *Mon. Wea. Rev.*, accepted.
- Kuhlman, K., C. Ziegler, E. Mansell, D. MacGorman, and J. Straka, 2006: Numerically simulated electrification and lightning of the 29 June 2000 STEPS supercell storm. *Mon. Wea. Rev.*, 134, 2734-2757.
- Krehbiel, P. R., R. J. Thomas, W. Rison, T. Hamlin, J. Harlin, and M. Davis, 2000: GPS-based mapping system reveals lightning inside storms. *Eos, Trans. Amer. Geophys. Union*, 81, 21-25. doi:10.1029/2004GL021802.
- MacGorman, D., W. D. Rust, P. Krehbiel, E. Bruning, and K. Wiens, 2005: The electrical structure of two supercell storms during STEPS. *Mon. Wea. Rev.*, 133, 2583-2607. *storm. J. Appl. Meteor.*, 14, 1521-1530.
- MacGorman, D., W. D. Rust, T. Schuur, M. Biggerstaff, J. Straka, C. Ziegler, E. Mansell, E. Bruning, K. Kuhlman, N. Lund, N. Biermann, C. Payne, L. Carey, P. Krehbiel, W. Rison, K. Eack, and W. Beasley, 2008: TELEX: The Thunderstorm Electrification and Lightning Experiment. *Bull. Amer. Meteor. Soc.*, 89, 997-1013, doi:10.1175/2007BAMS2352.1.
- Mansell, E., D. MacGorman, C. Ziegler, and J. Straka, 2002: Simulated three-dimensional branched lightning in a numerical thunderstorm model. *J. Geophys. Res.*, 107, 4075, doi:10.1029/2000JD000244.
- Mansell, E., ____, ____, and ____, 2005: Charge structure and lightning sensitivity in a simulated multicell thunderstorm. *J. Geophys. Res.*, 110, D12101, doi:10.1029/2004JD005287.
- Mansell, E., C. Ziegler, and E. Bruning, 2010: Simulated electrification of a small thunderstorm with two-moment bulk microphysics. *J. Atmos. Sci.*, 67, 171-194.
- Mansell, E., and Ziegler, C., 2013: Aerosol effects on simulated storm electrification and precipitation in a two-moment bulk microphysics model. *J. Atmos. Sci.*, 70, 2032-2050.
- Payne, C., T. Schuur, D. MacGorman, M. Biggerstaff, K. Kuhlman, and W. D. Rust, 2010: Polarimetric and electrical characteristics of a lightning ring in a supercell storm. *Mon. Wea. Rev.*, 138, 2405-2425.
- Steiger, S., R. Orville, and L. Carey, 2007: Total lightning signatures of thunderstorm intensity. Part I: Supercells. *Mon. Wea. Rev.*, 135, 3281-3302.
- Ziegler, C., D. MacGorman, J. Dye, and P. Ray, 1991: A model evaluation of non-inductive graupel-ice charging in the early electrification of a mountain thunderstorm. *J. Geophys. Res.*, 96, 12,833-12,855.
- Ziegler, C., and D. MacGorman, 1994: Observed lightning morphology relative to modeled space charge and electric field distributions in a tornadic storm. *J. Atmos. Sci.*, 51, 833-851.
- Ziegler, C., E. Mansell, D. MacGorman, and D. Burgess, 2007: Impact of varying inversion strength on the electrification, lightning, kinematics, and microphysics of a simulated supercell storm. *Preprints*, 13th International Conference on Atmospheric Electricity, Beijing, China, 4 pp.
- Ziegler, C., E. Mansell, J. Straka, D. MacGorman, and D. Burgess, 2010: The impact of spatial variations of low-

level stability on the life cycle of a simulated supercell storm. *Mon. Wea. Rev.*, **138**, 1738-1766, doi: 10.1175/2009MWR3010.1.